Quality assessment of reconstruction and relighting from RTI images: application to manufactured surfaces

Abir Zendagui[1], Jean-Baptiste Thomas[2], Gaëtan Le Goïc [1], Yuly Castro[1],
Marvin Nurit[1], Alamin Mansouri [1], Marius Pedersen[2]
[1]Imagerie et Vision Artificielle Laboratory, UFR Sciences et Techniques, University of Burgundy, Dijon, France.
[2] The Norwegian Colour and Visual Computing Laboratory, Department of computer science, NTNU, Gjøvik, Norway
Email: abir_zendagui@etu.u-bourgogne.fr

***Abstract*—In this paper, we propose to evaluate the quality of the reconstruction and relighting from images acquired by a Reflectance Transformation Imaging (RTI) device. Three relighting models, namely the PTM, HSH and DMD, are evaluated using PSNR and SSIM. A visual assessment of how the reconstructed surfaces are perceived is also carried out through a sensory experiment. This study allows to estimate the relevance of these models to reproduce the appearance of the manufactured surfaces. It also shows that DMD reproduces the most accurate reconstruction/relighting to an acquired measurement and that a higher sampling density don't mean necessarily a higher perceptual quality.**

***Index Terms*—Reflectance Transformation Imaging, psychometric evaluation, relighting.**

I. Introduction

The inspection of the visual quality of manufactured surfaces is often performed in a sensory way, through a visual analysis of the surfaces realized by industrial experts [1]. Typically, the inspection consists in changing the product surface orientation to vary the angle of incidence of the light, which makes it possible to better show the possible local appearance anomalies on the inspected surfaces. To improve the results reproducibility and variability, and to evaluate the criticality of the anomalies, a trend is to try, through the implementation of instrumental measuring devices to bring to the experts an aid to the detection, the evaluation and the decision with regard to the quality of appearance of surfaces. Based on the measured data, the main idea is to provide the experts with local objective indicators (detection and evaluation of anomalies) and global indicators (as example, for the assessment of the appearance of a surface finishing process) correlated with the perception of surfaces. One of the approaches used increasingly frequently in the industry to respond to this objective is the Reflectance Transformation Imaging technique (RTI). This Non Destructive Inspection (NDI) method consists in measuring the angular component of the reflectance, and simplifies the inspection conditions since only light position changing is to be considered. This technique is widely used for image relighting, i.e. for reconstructing a scene under an arbitrary (virtual) direction of illumination with applications in Video-games, Cultural heritage [2]–[6] and recently in manufacturing [7]–[9]. The RTI acquisition process consists in acquiring a set of images with a fixed camera generally positioned orthogonally to the inspected surface, while varying the light direction at each image capture. From this set of images, each pixel is associated a set of discrete values (measured gray-levels, considered to be proportional to the luminance [10]). To model the surface visual appearance continuously and to allow relighting the surface for any virtual direction of light, this set of luminance values can be approximated or interpolated locally [4], [11], [12]. The main approximation methods used to model this information are the Polynomial Texture Mappings approach (PTM), based on 2nd order polynomial functions [13], the Hemispherical Harmonics (HSH) approach [14] and the Discrete Modal Decomposition (DMD) [8], [15]–[17].
In this study, we investigates the accuracy of the reconstruction/relighting from RTI images using these three models (PTM, HSH, DMD). The quality of reconstruction is first assessed through objective indicators, by using the Peak Signal to Noise Ratio (PSNR) and Structural Similarity error metric (SSIM) [18]. Then, a subjective assessment is performed by implementing a psychometric experiment to compare the reconstruction quality in a perceptual way. The influence of the acquisition sampling density is also evaluated. Thus, the objective is to determine both the most appropriate method and the optimal RTI acquisition parameters to maximize correlation with visual perception of surfaces.

II. Background

The Reflectance Transformation Imaging (RTI) technique consists in acquiring stereo-photometric images. The light position is changed for each acquisition according to two directions $(\phi; \theta)$, allowing to change the incidence (respectively elevation and azimuth) of the light on the inspected surface. The sensor is generally positioned orthogonally to the surface to be acquired. For each pixel, a vector containing gray-level values associated to the different light positions used during

Agence Nationale de la Recherche through SUMUM and NAPS projects, The Norwegian Colour and Visual Computing Laboratory - NTNU

978-1-7281-5686-6/19/$31.00 ©2019 IEEE
DOI 10.1109/SITIS.2019.00121

the acquisition stage is obtained. These values are considered to be proportional to the luminance of the pixel [10], as described in equation 1, where k stands for the proportionality factor and $L(U_c)$ the associated luminance value.

$$G = k * L(U_c) \tag{1}$$

From these discrete luminance data, an experimental model is constructed in each pixel to describe with continuous functions the local angular reflectance. This operation is performed by realizing a least square (LS) regression of the luminance point cloud, from reference functions, called basis functions or projection basis functions. Different basis functions have been implemented in the literature to model the angular reflectance. The historical method, developed by Malzbender in 2001, implemented 2nd order polynomial functions. This method called Polynomial Texture Mappings showed limits to describe non-Lambertian complex reflectance behaviours. Thus, other families of approximation functions have been proposed, such as hemispherical harmonics (HSH technique) or more recently a family based on geometric shapes deriving from dynamic mechanics (DMD technique). The study proposed in this paper focuses on these 3 most often used techniques to model RTI data today. The principle of these 3 methods is detailed below.

Polynomial Texture Mapping (PTM). This technique was developed initially to improve the photo-realistic rendering in 3D imaging [13]. Widely used for cultural heritage applications [19], the PTM approach approximate the luminance surface in each pixel by a polynomial regression of 6 vectors $(a_0 - a_5)$. These 6 vectors are sought for each pixel from the quadratic surface representing the reflectance defined by equation 2

$$L(l_u, l_v) = a_0 + a_1 l_u + a_2 lv + a_3 l_u l_v + a_4 l_u^2 + a_5 l_v \tag{2}$$

As indicated previously, the equation 2 is solved by a LS regression. The simplicity of the functions that constitute the projection basis (2nd order polynomials) does not make it possible to describe complex reflectances. However, this method - easy to implement and quick- demonstrates its efficiency when a small stack of images is acquired, and for lambertian surfaces.

Hemispherical Harmonics (HSH). The HSH is an improvement of the PTM technique [20] that implements more complex basis functions [21], [22] derived from Hemispherical harmonics. Gautron et al. defined the hemispheric harmonic bases $H_l^m(\theta, \phi)$ as an adapted version of spherical harmonies $S_l^m(\theta, \phi)$ that rely on derivation of Legendre polynomials (3). These functions allow a finer description of the local reflectance behaviour of the surfaces, in particular when angular variations of lighting are associated with rapid and large amplitude of luminance.

$$P_l^m(cos\theta) = P_l^m(2cos\theta - 1) \; and \; \theta \in \left[0, \frac{\pi}{2}\right] \tag{3}$$

Discrete Modal Decomposition (DMD). The DMD is a technique initially used in dynamic mechanics to decompose a vibration. Then it has been implemented for geometrical tolerancing [23], multi-scale analysis of topographic surface roughness[24], [25] and for heat source evaluation [26]. This method was then adapted and implemented in the field of visual appearance [8], [15], [16], to model the local behaviour of the reflectance angular component at each point/pixel. The DMD technique consists in decomposing the signal (*i.e* in the case of the appearance the discrete luminance values associated to each pixel into a family of functions named eigen-modes, associated to the natural modes of vibration of a reference structure (that can be a plane, a cylinder, or an hemispheric form). These natural modes form the projection basis, named the modal basis. Thus, the modal modes derives from the resolution of the dynamic equation (4).

$$K.q + M.q^{"} = 0 \tag{4}$$

$$\text{With} \quad q = q(x, y, t) = \sum_{i=1}^{+\infty} Q_i(x, y).cos(\omega_i t) \tag{5}$$

Where M is the Mass matrix, K is the stiffness matrix and $q(x, y, t)$ is the displacements that characterizes the modal shapes. The projection of the measured surface onto the modal basis is then the sum of a linear combination of modal vectors and the decomposition residual (6)

$$V = \sum_{i=1}^{N_q} \lambda_i Q_i + \epsilon(N_q) \tag{6}$$

With Q_i is the modal vectors composing the modal basis. λ_i is the modal coordinates and N_q is the number of modes of decomposition. An example of reconstruction results for the same pixel using the three approximations PTM, HSH and DMD are presented in Figure 1.

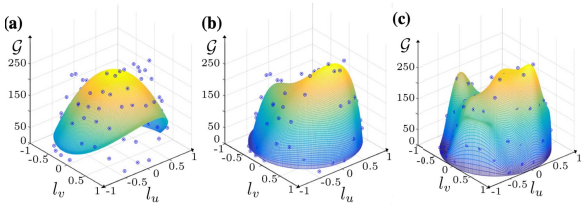

Fig. 1. Example of the reconstruction of the same pixel (metallic engineered surface) using from left to right PTM, HSH and DMD technique, from [8]

III. Proposed Evaluation

A. RTI Acquisition device

The home-made RTI acquisition (see Figure 2) device we used in this study is built in a manner to allow the positioning of the light source precisely for any incidence angles $(\theta; \phi)$. The light source is fixed on a rotated motorized hoop, that allows to construct a virtual lightening dome around the surface with flexible positioning of the light source. The

camera and the lenses were chosen to ensure high quality and high resolution images.

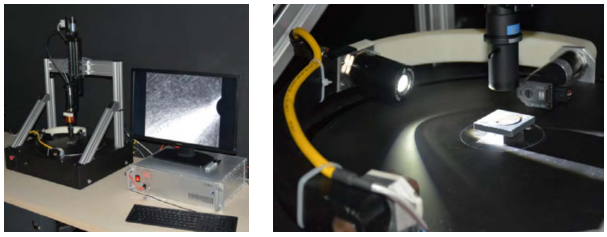

Fig. 2. RTI acquisition device

B. Samples

The manufactured surfaces used in this study are ten metallic sides of industrial manufactured rings. These surfaces, referred as LGR in this paper, were polished by a tribofinition finishing process composed successively of softening, polishing and brightening operations. The ten rings are associated to five process groups: the difference between groups is the softening time, varying from 40 to 80 minutes, which induces a surface roughness varying from 0.22 to $0.17\mu m$.

To build our dataset for the experiment, a dense RTI acquisition was acquired (650 measurements - $(130\times\theta; 5\times\phi)$) on different plane surfaces of the parts. The resolution of the images is 512×700 pixels, which corresponds to an approximate pixel size of 1.5 μm^2. A higher acquisition density (in the angular space) has been chosen for the θ axis. This choice is related to the experience gained in previous RTI studies, where it was observed that for flat-shaped surfaces, the information obtained by varying the θ angle was much more discriminating than the information obtained by varying ϕ illumination angle. Moreover, the variation associated with a variation of the angle ϕ often being close enough to what would have been obtained by varying the intensity of the source. On the RTI device used, the objective is close to the surface (approximately 30 mm) to perform RTI measurements at this magnification. This induces an angular limitation on the ϕ axis, the blind area corresponds to ϕ values greater than approximately $60°$. In this study, to avoid the risk of contact between the source and the sensor during RTI acquisitions, the elevation angle was limited to $55°$.

For reconstruction models, the contributions are calculated with 6 terms for PTM, 9 harmonics for HSH and 50 modes for DMD. To estimate the visual quality of the RTI-based reconstructions, the direction of the virtual lighting used is the same for the measured image, see example in Figure 4. Five reconstruction light directions were chosen: $(\theta : 180°, \phi : 14.5°), (\theta : 180°, \phi : 28°), (\theta : 180°, \phi : 41.5°), (\theta : 180°, \phi : 55°), (\theta : 180°, \phi : 14.5°), (\theta : 88.6154°, \phi : 41.5°)$.

C. Objective evaluation

The first metric we used for the objective evaluation is the Peak Signal to Noise Ratio (PSNR) since it has already proven its relevance in RTI data. The PSNR has been used to evaluate the efficiency of the fitting models for reflectance reconstruction [8], [12], [15], to evaluate RTI compressed images quality visualised on a mobile device [27], or for web relighting tools [28] In this study, we propose to use this metric in order to to investigate its correlation with subjective assessments of how surfaces are perceived, and therefore evaluate the the quality of the reconstruction models in a perceptual sense [15].

Fig. 3. Samples of the study (Industrial manufactured rings)

PSNR results are presented in Table II. The PSNR is evaluated for the reconstructed images using the three reconstruction models, and compared to the PSNR of the reference image, *i.e.* the acquisition image at the same angle in which the reconstruction was performed, and for different acquisition sampling density (All, Half, Fifth, Seventh). The images were reconstructed at 5 different light incidence angles to vary the configurations in terms of exposure and shade. Table III presents the PSNR results computed over the 5 surface groups, using DMD reconstruction and varying sampling densities.

Then, we implement in this study the Sturctural Similarity metric index (SSIM), in order to take in consideration the spatial aspect, and thus to have a criterion closer to perception than the PSNR. In the same manner of the PSNR, the SSIM is computed on the reconstructions using the 3 approximation models, different sampling density, and for five light directions (see Table VII). Table VIII presents the SSIM results computed over the 5 surface groups, using DMD reconstruction and varying sampling densities.

Finally, statistics are computed (see Table V) to assess and rank the approximation models, and to evaluate the influence of the acquisition sampling density when reconstructing with DMD (Table VI).

TABLE I
GLOBAL MEAN AND MEDIAN OF PSNR

Method	Mean	Median
PTM	17.46	19.46
HSH	24.52	23.47
DMD	26.76	25.67

D. Results and discussion

It is observed in Table I that significant differences are obtained in terms of PSNR global mean and median. According

TABLE II
PSNR OF IMAGE RECONSTRUCTIONS USING PTM, HSH, DMD AND DIFFERENT SAMPLING DENSITIES

Sampling	Angle	PTM	HSH	DMD
All (1): 650 position	$\theta : 180°, \phi : 14.5°$	12,13	31,06	34,87
	$\theta : 180°, \phi : 28°$	20,65	26,17	29,11
	$\theta : 180°, \phi : 41.5°$	19,46	22,64	25,43
	$\theta : 180°, \phi : 55°$	14,90	19,52	22,37
	$\theta : 88.61°, \phi : 41.5°$	20,26	23,60	26,06
Half (1/2): 324 position	$\theta : 180°, \phi : 14.5°$	12,10	31,03	34,84
	$\theta : 180°, \phi : 28°$	20,66	26,17	28,83
	$\theta : 180°, \phi : 41.5°$	19,47	22,66	25,53
	$\theta : 180°, \phi : 55°$	14,87	19,51	22,23
	$\theta : 88.61°, \phi : 41.5°$	20,26	23,57	25,82
Fifth (1/5): 130 position	$\theta : 180°, \phi : 14.5°$	12,09	30,91	33,62
	$\theta : 180°, \phi : 28°$	20,66	26,28	30,14
	$\theta : 180°, \phi : 41.5°$	19,47	22,63	24,69
	$\theta : 180°, \phi : 55°$	14,89	19,60	22,99
	$\theta : 88.61°, \phi : 41.5°$	20,25	23,37	24,21
Seventh (1/7): 93 position	$\theta : 180°, \phi : 14.5°$	12,10	**30,78**	**30,37**
	$\theta : 180°, \phi : 28°$	20,59	**25,83**	**25,89**
	$\theta : 180°, \phi : 41.5°$	19,42	22,50	24,42
	$\theta : 180°, \phi : 55°$	14,80	19,31	20,60
	$\theta : 88.61°, \phi : 41.5°$	20,25	**23,29**	**23,20**

TABLE III
PSNR OF IMAGE RECONSTRUCTIONS USING DMD AND DIFFERENT SAMPLING DENSITIES

Surfaces	Angles	ALL	HALF	FIFTH	SEVEN
Surface 1:A01	$(180°, 14.5°)$	34,87	34,84	33,62	30,37
	$(180°, 28°)$	29,11	28,83	**30,14**	25,89
	$(180°, 41.5°)$	25,43	25,53	**24,69**	24,42
	$(180°, 55°)$	22,37	22,23	**22,99**	20,60
	$(88.61°, 41.5°)$	26,06	25,82	24,21	23,20
Surface 2: A04	$(180°, 14.5°)$	36,10	36,05	34,80	31,52
	$(180°, 28°)$	31,14	30,84	**32,26**	27,92
	$(180°, 41.5°)$	27,29	**27,38**	26,76	26,30
	$(180°, 55°)$	23,75	23,61	**24,55**	21,69
	$(88.61°, 41.5°)$	24,71	24,48	22,81	21,86
Surface 3: A06	$(180°, 14.5°)$	35,21	35,15	34,09	30,90
	$(180°, 28°)$	30,64	30,39	**31,45**	27,26
	$(180°, 41.5°)$	27,96	**28,04**	27,14	26,93
	$(180°, 55°)$	24,74	24,59	**25,35**	22,63
	$(88.61°, 41.5°)$	23,56	23,30	21,73	20,65
Surface 4: A07	$(180°, 14.5°)$	36,37	36,31	35,15	31,55
	$(180°, 28°)$	30,32	29,98	**31,61**	27,40
	$(180°, 41.5°)$	26,76	**26,88**	26,17	25,85
	$(180°, 55°)$	23,59	23,41	**24,48**	21,60
	$(88.61°, 41.5°)$	26,01	25,68	24,17	23,17
Surface 5: A10	$(180°, 14.5°)$	37,20	37,16	35,83	32,63
	$(180°, 28°)$	31,88	31,47	**32,58**	28,51
	$(180°, 41.5°)$	27,49	**27,60**	26,50	26,00
	$(180°, 55°)$	23,35	23,14	**23,98**	21,53
	$(88.61°, 41.5°)$	26,58	26,28	24,86	23,94

to this criterion, the DMD method appears to be more efficient than HSH and PTM based reconstructions. However, according to the quantitative metrics (PSNR and SSIM) implemented, it can be noticed that the differences are less significant when using 1/7 sampling density (see Table II), where for example HSH and DMD have a score of respectively 30.78 and 30.37 for $(\theta : 180°, \phi : 14.5°)$; 25.83, 25.89 for $(\theta : 180°, \phi : 28°)$; and 23.29, 23.20 for $(\theta : 88.61°, \phi : 41.5°)$. Analog results are obtained using SSIM citerion (Table VII). Regarding the quality of reproductions using DMD over the 5 manufactured surfaces using PSNR (Table III) and SSIM (Table VIII), the higher score is obtained with a $1/5$ sampling density for two light directions $(\theta : 180°, \phi : 28°)$ and $(\theta : 180°, \phi : 55°)$, that indicates that a higher quality of reproduction is obtained with this sampling density for these two directions. In addition, for the light direction associated to $(\theta : 180°, \phi : 41.5°)$ (see Table VIII), the $1/2$ sampling density stands out in terms of both SSIM and PSNR for the five surface groups.

The results using both PSNR and SSIM show that the DMD technique outperforms the other models when reconstructing the angular reflectance and that the acquisition sampling density is of primary importance. However, as shown in [8], althought calculated locally, PSNR and SSIM express an average metric, which is often not relevant to describe salient features of a surface, or singular local behaviors, which are of primary importance for the human when discriminating, and more generally evaluating the appearance of two surfaces. This means that the spatial aspects witch are fundamental in human sensory assessments and in terms of perception are not taken into account. Thus, a further psychometric experiment is proposed in this study in order to evaluate subjectively the perceived quality of the RTI-based surface appearance reconstructions. This second part of the study, and the associated results are presented in section III-E.

TABLE IV
PSNR GLOBAL MEAN AND MEDIAN COMPUTED USING DIFFERENT SAMPLING DENSITIES

Method	ALL	HALF	FIFTH	SEVENTH
Mean	28.29	28.16	27.86	25.57
Median	27.02	27.13	26.33	25.82

TABLE V
SSIM GLOBAL MEAN AND MEDIAN COMPUTED IN 5 DIFFERENT LIGHT DIRECTIONS

Method	Mean	Median
PTM	0.37	0.42
HSH	0.65	0.67
DMD	0.73	0.73

TABLE VI
SSIM GLOBAL MEAN AND MEDIAN COMPUTED USING DIFFERENT SAMPLING DENSITIES

Method	ALL	HALF	FIFTH	SEVENTH
Mean	0.77	0.76	0.74	0.64
Median	0.76	0.77	0.72	0.68

E. Visual sensory assessment

To evaluate the performance of the reconstruction models, *i.e.* in this study the PTM, HSH and DMD (see Figure 4), to reproduce visual appearance of manufactured surfaces, a psychometric experiment was Implemented. This experiment has two main objectives: (i) determine the impact of the fitting

TABLE VII
SSIM OF IMAGE RECONSTRUCTIONS USING PTM, HSH, DMD AND DIFFERENT SAMPLING DENSITIES

Sampling	Angle	PTM	HSH	DMD
All (1): 650 position	$\theta : 180°, \phi : 14.5°$	0,17	0,70	0,88
	$\theta : 180°, \phi : 28°$	0,42	0,71	0,83
	$\theta : 180°, \phi : 41.5°$	0,49	0,68	0,76
	$\theta : 180°, \phi : 55°$	0,34	0,54	0,66
	$\theta : 88.61°, \phi : 41.5°$	0,46	0,66	0,75
Half (1/2): 324 position	$\theta : 180°, \phi : 14.5°$	0,17	0,70	0,88
	$\theta : 180°, \phi : 28°$	0,42	0,71	0,82
	$\theta : 180°, \phi : 41.5°$	0,49	0,68	0,77
	$\theta : 180°, \phi : 55°$	0,33	0,54	0,64
	$\theta : 88.61°, \phi : 41.5°$	0,46	0,65	0,73
Fifth (1/5): 130 position	$\theta : 180°, \phi : 14.5°$	0,17	0,69	0,84
	$\theta : 180°, \phi : 28°$	0,42	0,71	0,84
	$\theta : 180°, \phi : 41.5°$	0,48	0,66	0,70
	$\theta : 180°, \phi : 55°$	0,33	0,56	0,72
	$\theta : 88.61°, \phi : 41.5°$	0,45	0,63	0,64
Seventh (1/7): 93 position	$\theta : 180°, \phi : 14.5°$	0,16	0,69	0,74
	$\theta : 180°, \phi : 28°$	0,41	**0,68**	**0,69**
	$\theta : 180°, \phi : 41.5°$	0,48	**0,66**	**0,69**
	$\theta : 180°, \phi : 55°$	0,31	**0,50**	**0,51**
	$\theta : 88.61°, \phi : 41.5°$	0,45	**0,62**	**0,59**

TABLE VIII
SSIM OF IMAGE RECONSTRUCTIONS USING DMD AND DIFFERENT SAMPLING DENSITIES

Surfaces	Angles	ALL	HALF	FIFTH	SEVEN
Surface 1:A01	$(180°, 14.5°)$	0,88	0,88	0,84	0,74
	$(180°, 28°)$	0,83	0,82	**0,84**	0,69
	$(180°, 41.5°)$	0,76	**0,77**	0,70	0,69
	$(180°, 55°)$	0,66	0,64	**0,72**	0,51
	$(88.61°, 41.5°)$	0,75	0,73	0,64	0,59
Surface 2: A04	$(180°, 14.5°)$	0,88	0,88	0,84	0,74
	$(180°, 28°)$	0,84	0,82	**0,86**	0,70
	$(180°, 41.5°)$	0,76	**0,77**	0,71	0,69
	$(180°, 55°)$	0,65	0,63	**0,72**	0,49
	$(88.61°, 41.5°)$	0,69	0,66	0,56	0,50
Surface 3: A06	$\theta : 180°, 14.5°)$	0,84	0,84	0,80	0,72
	$(180°, 28°)$	0,84	0,82	**0,84**	0,70
	$(180°, 41.5°)$	0,79	**0,80**	0,73	0,71
	$(180°, 55°)$	0,68	0,66	**0,73**	0,53
	$(88.61°, 41.5°)$	0,68	0,65	0,56	0,50
Surface 4: A07	$(180°, 14.5°)$	0,90	0,89	0,85	0,76
	$(180°, 28°)$	0,85	0,83	**0,86**	0,71
	$(180°, 41.5°)$	0,75	**0,76**	0,69	0,67
	$(180°, 55°)$	0,64	0,61	**0,72**	0,48
	$(88.61°, 41.5°)$	0,71	0,67	0,58	0,53
Surface 5: A10	$(180°, 14.5°)$	0,91	0,90	0,87	0,79
	$(180°, 28°)$	0,86	0,84	**0,87**	0,73
	$(180°, 41.5°)$	0,76	**0,77**	0,69	0,66
	$(180°, 55°)$	0,63	0,59	**0,71**	0,47
	$(88.61°, 41.5°)$	0,76	0,73	0,66	0,62

models on the surface appearance reconstruction (ii) determine the impact of the sampling density.

1) Controlled psychometric experiment: The psychometric experiment is carried out on a dedicated web-based platform designed for psychometric scaling experiments (QuickEval [29]). In order to increase the perceived contrast of images with the environment, a black background was picked-out for the web-page and the experiment held in a dark room (no lighting with matt grey wall). The experiment is a paired comparison [30] where participants' task is to choose the most

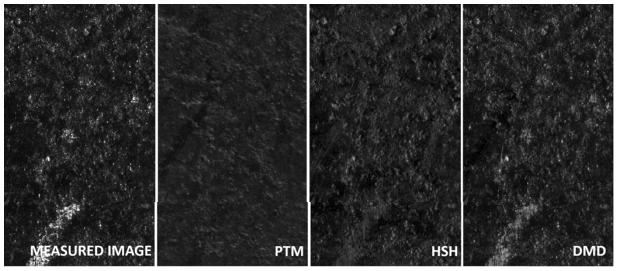

Fig. 4. Example of a measured image and RTI-based reconstructions in lighting direction $(\theta : 180°, \phi : 41.5°)$

similar representation (the reconstructed images using two of the three fitting models each time, positioned on the left and on the right) to the original image (the acquired image positioned in the middle). The experiment was setup as a forced-choice experiment with flipping of the pairs. The experiment divided on two parts took in average 30 minutes (10 minutes for the 1^{st} part and 20 minutes for the 2^{nd} part) for 240 comparison in total. The two parts answer respectively to the main goals presented previously.

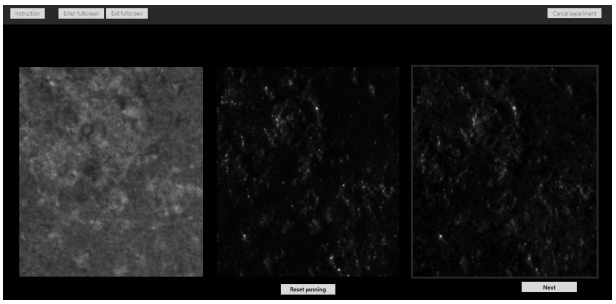

Fig. 5. Screen shot of the QuickEval experiment platform, in the center the original image, in left and right two reconstruction images at the same light angle

2) Participants: The participants involved in this experiment were 19 volunteer researchers working at the Norwegian Colour and Visual Computing Laboratory. They can be considered as experienced observers in psychometric experiments.

F. Results and discussion

Results in terms of users' preferences comparing the three approximation models are presented in Figure 6. The five groups of the graph are according to the chosen five angles for the experiment. It is observed that more than 60% of the users picked out DMD as the more accurate reproduction to the reference shown (raw image) while roughly 30% of them chose HSH reconstructions. We make the assumption that this amount of HSH votes is due to cases where the choice is difficult because the reconstructed images are either very similar, or both very different from the reference. Concerning the PTM choices (6% of user's preferences corresponding to angles $(\theta : 180°, \phi : 14.5°)$ whithout sampling, and 1%

corresponding to the same angle but $1/7$th sampling, our interpretation is that this is due to poorness of PTM to approximate the luminance of the pixel. The consequence is that it produces an average of the pixel's luminance under exposed $(\theta : 180°, \phi : 14.5°)$ and overexposed $(\theta : 180°, \phi : 55°)$, which can be favourable in terms of perception, in some very particular light configurations. It is observed in addition that the PTM for $(\theta : 88.6154°, \phi : 41.5°)$ produces better reconstruction results (see Figure 7) comparing to the results obtained with other sampling densities, which confirms that PTM can be an appropriate method when a low number of images are acquired in an RTI acqusition. These results

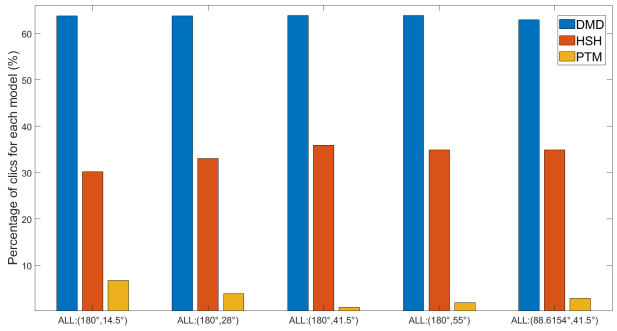

Fig. 6. Number of times a reproduction has been selected using the three fitting models : DMD, HSH, PTM whithout sampling

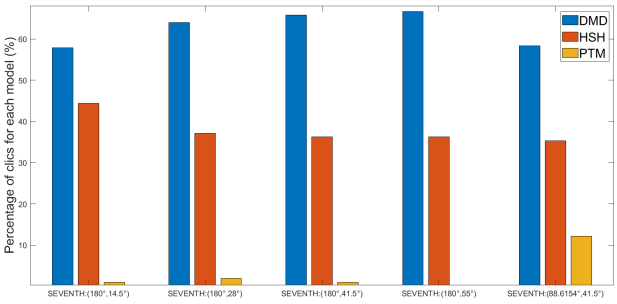

Fig. 7. Number of times a reproduction has been selected using the three fitting models : DMD, HSH, PTM with $1/7$th sampling

are detailed and extended in Table IX for all the angles and sampling density used in the study, where the standard deviation to the mean is ~ 2 for DMD in 75% of cases which makes it two standard deviation better than the average of the votes. And $\sim$ -2 for PTM in 75% of cases. In the other cases, and as explained before the gap between the performance of models decreases with less measurements and increases in some angles (phi = $14.5°$ and $55°$).

The Table XI shows that the global mean and median of all the tested cases in the experiment, rank the accuracy of the reproduced images as PTM for the worst similarity to the original image, then HSH and DMD stands out as the most accurate method for the reconstruction of the visual apperance on these surfaces. This conclusion matches with previous results obtained using the objective quality metrics (PSNR and SSIM). The second part of the experiment was devoted

TABLE IX
Z-SCORE FOR THE REPRODUCED IMAGES USING PTM, HSH, DMD AND 4 SAMPLING DENSITY (ALL, HALF, FIFTH AND SEVENTH) WITH THE ACQUIRED IMAGES IN DIFFERENT ANGLES

Sampling	Angle	PTM	HSH	DMD
All (1): 650 position	$\theta : 180°, \phi : 14.5°$	-1,77	0,52	2,29
	$\theta : 180°, \phi : 28°$	-1,94	0,34	2,28
	$\theta : 180°, \phi : 41.5°$	-2,28	0,00	2,28
	$\theta : 180°, \phi : 55°$	-2,12	0,16	2,28
	$\theta : 88.61°, \phi : 41.5°$	-2,02	0,10	2,13
Half (1/2): 324 position	$\theta : 180°, \phi : 14.5°$	-2,28	0,34	1,94
	$\theta : 180°, \phi : 28°$	-2,02	0,26	2,28
	$\theta : 180°, \phi : 41.5°$	-2,02	0,10	2,13
	$\theta : 180°, \phi : 55°$	0,00	0,00	0,00
	$\theta : 88.61°, \phi : 41.5°$	-2,12	0,50	2,62
Fifth (1/5): 130 position	$\theta : 180°, \phi : 14.5°$	-2,13	0,10	2,02
	$\theta : 180°, \phi : 28°$	-2,12	0,16	2,28
	$\theta : 180°, \phi : 41.5°$	-2,02	0,10	2,13
	$\theta : 180°, \phi : 55°$	-2,65	0,62	2,03
	$\theta : 88.61°, \phi : 41.5°$	-2,13	0,10	2,02
Seventh (1/7): 93 position	$\theta : 180°, \phi : 14.5°$	-2,28	0,65	1,63
	$\theta : 180°, \phi : 28°$	-2,13	0,10	2,02
	$\theta : 180°, \phi : 41.5°$	-2,28	0,00	2,28
	$\theta : 180°, \phi : 55°$	0,00	0,00	0,00
	$\theta : 88.61°, \phi : 41.5°$	-1,16	0,12	1,30

TABLE X
GLOBAL MEAN AND MEDIAN OF Z-SCORE COMPUTED OVER 5 REPRODUCED SURFACES' ASPECT IN 5 LIGHT DIRECTIONS

Method	Mean	Median
PTM	-1.87	-2.12
HSH	-0.02	-0.05
DMD	1.90	2.13

to study the impact of the sampling density as explained in III-E1. Considering the number of times a reconstruction has been selected in Figure 8 computed using one surface and roughly the same result for the other four surfaces, we notice that more measurements does not mean necessarily a better visual aspect. In the grazing angle $(\theta : 180°, \phi : 14.5°)$ a higher sampling density where chosen: ALL= 30% of votes, HALF= 30%, FIFTH=30% as a higher quality representation of the original image. This ranking is changed for other angles (higher elevation) and less density of measurements is more accurate to the acquired image, 45% of votes were for the lower density $(1/7)$ for the three angles and less than 15% for the highest sampling density. This is due to the extra perceived information that RTI provides to the image by integrating in computing the pixels' luminance for one angle, the luminance of the pixel in all lighting directions. And since the task of users is to choose the closer representation to the reference, the extra information can in some cases disturbs their perceptual evaluation of the reconstructed images.

The results of mean z-score for the five angles and the five surfaces chosen for the experiment is presented in Table XII. For the different sampling density tested, the standard deviation to the mean is higher for a $1/7$ of the measurements

for the three angles ($\theta : 180°, \phi : 41.5°$),($\theta : 180°, \phi : 55°$),($\theta : 88.61°, \phi : 41.5°$) for all the surfaces. A full measurements density were preferred for a lower elevation ($\theta : 180°, \phi : 28°$),($\theta : 180°, \phi : 14.5°$) because in these angles, images are dark, so the perceptual evaluation is biased due to the limitation of the sensor which represent the values of pixel in only 1 byte. A future improvement of this investigation is to extend our acquisition to be able to build high dynamic range images. Computing the the global mean of the z-score in Table XI for all the surfaces and the angles for each density ranks the quality of the reconstructed images using different sampling density respectively as: All, Half, Fifth and the seventh from the worst to the best perceived quality.

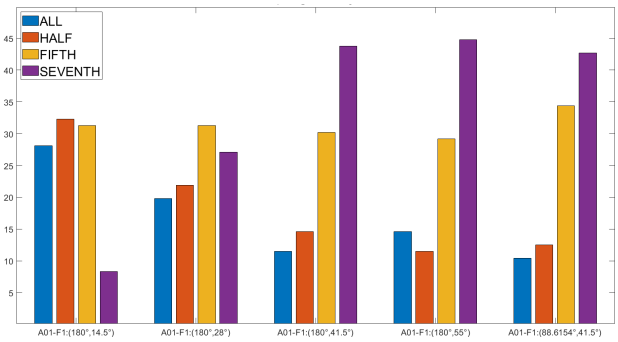

Fig. 8. Number of times a reproduction has been selected using four sampling density : All, Half, Fifth and a Seventh of the measurement using one of the five manufactured surfaces: A01

TABLE XI
GLOBAL MEAN AND MEDIAN OF Z-SCORE COMPUTED OVER 5 REPRODUCED SURFACES' ASPECT IN 5 LIGHT DIRECTIONS USING DIFFERENT SAMPLING DENSITIES

Method	ALL	HALF	FIFTH	SEVENTH
Mean	-0.65	-0.43	0.50	0.58
Median	-0.77	-0.56	0.48	0.89

IV. CONCLUSION

The study presented in this paper aims to evaluate the quality of the reconstruction and relighted images using RTI stereo photo-metric images. The reconstruction models used: PTM, HSH, DMD with different sampling densities. The evaluation of the relighted images is done first with objective error metrics: PSNR and SSIM and second with psychometric experiment to involve the human subjective evaluation of surfaces as a reference for the perceptual evaluation of manufactured surfaces aspect. The subjective and objective evaluation of the surfaces' aspect shows that DMD outperforms PTM and HSH as a the most accurate model to approximate the perceptual aspect of a surface. The results of the objective metrics show also the inefficiency of these metrics to evaluate the perceptual quality of surfaces using the RTI protocol. Results of the evaluation shows also that the quality of the reconstruction using RTI-based images can decrease with a high sampling

TABLE XII
Z-SCORE FOR THE REPRODUCED IMAGES USING DMD AND 4 SAMPLING DENSITY (ALL, HALF, FIFTH AND SEVENTH) WITH THE ACQUIRED IMAGES IN DIFFERENT ANGLES FOR THE FIVE SURFACES.

Surfaces	Angles	ALL	HALF	FIFTH	SEVEN
Surface 1:A01	$(180°, 14.5°)$	0,19	**0,41**	0,38	**0,97**
	$(180°, 28°)$	0,27	0,16	**0,32**	0,11
	$(180°, 41.5°)$	0,75	0,73	0,30	**1,19**
	$(180°, 55°)$	0,63	-1,04	0,22	**1,44**
	$(88.61°, 41.5°)$	0,95	-1,01	0,57	**1,38**
Surface 2: A04	$(180°, 14.5°)$	0,67	**0,17**	**0,35**	-1,19
	$(180°, 28°)$	0,68	**0,16**	**0,51**	0,34
	$(180°, 41.5°)$	0,91	-1,04	0,30	**1,66**
	$(180°, 55°)$	-1,06	0,52	0,67	**0,90**
	$(88.61°, 41.5°)$	0,68	0,89	0,67	**0,90**
Surface 3: A06	$(180°, 14.5°)$	0,49	**0,11**	**0,46**	-1,06
	$(180°, 28°)$	0,35	0,51	**0,75**	0,11
	$(180°, 41.5°)$	-1,00	0,92	0,73	**1,19**
	$(180°, 55°)$	-1,12	0,84	0,38	**1,57**
	$(88.61°, 41.5°)$	-1,00	0,79	0,51	**1,28**
Surface 4: A07	$(180°, 14.5°)$	0,38	**0,67**	0,06	-1,12
	$(180°, 28°)$	0,78	0,44	**0,95**	0,27
	$(180°, 41.5°)$	0,97	**0,38**	**0,52**	**0,84**
	$(180°, 55°)$	-1,19	0,69	0,38	**1,50**
	$(88.61°, 41.5°)$	**0,87**	0,66	0,66	**0,87**
Surface 5: A10	$(180°, 14.5°)$	0,05	0,49	0,34	0,77
	$(180°, 28°)$	0,83	0,16	0,71	0,28
	$(180°, 41.5°)$	-1,28	0,89	0,73	**1,44**
	$(180°, 55°)$	-1,37	0,58	0,38	**1,57**
	$(88.61°, 41.5°)$	-2,01	0,66	1,09	**1,70**

angular density. This disturbance of the perceived quality is induced by the fact that the models used (PTM, HSH, DMD) are global and therefore non-interpolating. The approximation obtained in each pixel therefore corresponds to an integration of the discrete information acquired for this pixel. In the case of dense acquisitions, this can lead to the appearance of details which are associated with nearby lighting directions, therefore not visible in the reference raw acquisition image, which are detrimental to perception.

REFERENCES

[1] A. S. Guerra, "Métrologie sensorielle dans le cadre du contrôle qualité visuel," PhD thesis, Laboratoire Symme - Université de Savoie, 2009.

[2] H. Pagi, J. Miles, A. Uueni, S. Hogarth, and K. Sikka, "Reflectance Transformation Imaging in Daguerreotype Investigation," *ingentaconnect.com*, vol. 2017, no. 1, pp. 116–121, May 2017.

[3] D. Selmo, F. Sturt, J. Miles, P. Basford, T. Malzbender, K. Martinez, C. Thompson, G. Earl, and G. Bevan, "Underwater reflectance transformation imaging: a technology for in situ underwater cultural heritage object-level recording," *Journal of Electronic Imaging*, vol. 26, no. 1, p. 011 029, Feb. 2017.

[4] A. Giachetti, I. Ciortan, C. Daffara, R. Pintus, and E. Gobbetti, "Multispectral RTI analysis of heterogeneous artworks," 2017.

[5] I. Ciortan, R. Pintus, G. Marchioro, C. Daffara, and A. Giachetti, "A practical reflectance transformation imaging pipeline for surface characterization in cultural heritage," 2016.

[6] Y. Castro, G. Pitard, G. Le Goic, V. Brost, A. Mansouri, A. Pamart, J. M. Vallet, and L. De Luca, "A new method for calibration of the spatial distribution of light positions in free-form RTI acquisitions," vol. 11058, p. 1 105 813, 2019.

[7] G. Pitard, G. Le Goic, A. Mansouri, H. Favreliere, M. Pillet, S. George, and J. Y. Hardeberg, "Robust Anomaly Detection Using Reflectance Transformation Imaging for Surface Quality Inspection," *Scandinavian Conference on Image Analysis : Image Analysis*, vol. 10269, no. 1, pp. 550–561, Jun. 2017.

[8] G. Pitard, G. Le Goic, A. Mansouri, H. Favreliere, S.-F. Désage, S. Samper, and M. Pillet, "Discrete Modal Decomposition: a new approach for the reflectance modeling and rendering of real surfaces," *Machine Vision and Applications*, vol. 28, no. 5-6, pp. 607–621, Jul. 2017.

[9] G. Pitard, G. Le Goic, A. Mansouri, H. Favreliere, M. Pillet, S. George, and J. Y. Hardeberg, "Reflectance-based surface saliency," in *2017 IEEE International Conference on Image Processing (ICIP)*, IEEE, 2017, pp. 445–449.

[10] J. D. Durou, "Shape from shading – Eclairages, réflexions et perspectives," Tech. Rep., 2007.

[11] M. Zhang and M. S. Drew, "Efficient robust image interpolation and surface properties using polynomial texture mapping," *Eurasip Journal on Image and Video Processing*, pp. 1–36, 2014.

[12] R. Pintus, T. Dulecha, A. J. Villanueva, and A. Giachetti, "Objective and Subjective Evaluation of Virtual Relighting from Reflectance Transformation Imaging Data," 2018.

[13] T. Malzbender, D. Gelb, and H. Wolters, "Polynomial texture maps," *Proceedings of the 28th annual conference on Computer graphics and interactive techniques*, pp. 519–528, 2001.

[14] P. Gautron, J. Krivanek, S. N. Pattanaik, and K. Bouatouch, "A Novel Hemispherical Basis for Accurate and Efficient Rendering," *Eurographics Symposium on Rendering 2004*, pp. 1–10, 2004.

[15] G. Pitard, G. Le Goic, and H. Favreliere, "Discrete Modal Decomposition for surface appearance modelling and rendering," *SPIE Optical …*, 2015.

[16] G. Le Goic, "Qualité géométrique & Aspect des surfaces," PhD thesis, Université de Grenoble, Annecy, Oct. 2012.

[17] M. Nurit, Y. Castro, A. Zendagui, G. Le Goic, H. Favreliere, and A. Mansouri, "High dynamic range reflectance transformation imaging: an adaptive multi-light approach for visual surface quality assessment," in *International Conference on Quality Control by Artificial Vision (QCAV)*, International Society for Optics and Photonics, 2019, p. 1 117 213.

[18] Z. Wang, A. C. Bovik, H. S. I. t. on, and 2004, "Image quality assessment: from error visibility to structural similarity," *ece.uwaterloo.ca*,

[19] L. MacDonald and S. Robson, "Polynomial Texture Mapping and 3D representations," *International Archives of Photogrammetry, Remote Sensing and Spatial Information Sciences*, vol. 38, 2010.

[20] S. H. Westin, J. R. Arvo, and K. E. Torrance, "Predicting Reflectance Functions from Complex Surfaces," PhD thesis, Faculty of the Graduate School of Cornell University, 1992.

[21] P. Gautron, J. Krivanek, and S. N. Pattanaik, "A Novel Hemispherical Basis for Accurate and Efficient Rendering.," *Rendering …*, 2004.

[22] J. Kautz, P. P. Sloan, and J. Snyder, "Fast, arbitrary BRDF shading for low-frequency lighting using spherical harmonics," in *Proceedings of the 13th Eurographics Workshop on Rendering*, 2002.

[23] P. A. Adragna, S. Samper, F. Formosa, and M. Pillet, "Modal Tolerancing—Application to Gap and Flush Analyses," *Advances in Integrated Design and Manufacturing in Mechanical Engineering II*, pp. 417–430, 2007.

[24] G. L. Goic, H. Favreliere, S. Samper, and F. Formosa, "Multi scale modal decomposition of primary form, waviness and roughness of surfaces," *Scanning*, 2011.

[25] C. A. Brown, H. N. Hansen, X. J. Jiang, F. Blateyron, J. Berglund, N. Senin, T. Bartkowiak, B. Dixon, G. Le Goic, and Y. Quinsat, "Multiscale analyses and characterizations of surface topographies," *CIRP annals*, vol. 67, no. 2, pp. 839–862, 2018.

[26] T. Pottier, H. Louche, S. Samper, H. Favreliere, F. Toussaint, and P. Vacher, "Proposition of a modal filtering method to enhance heat source computation within heterogeneous thermomechanical problems," *International Journal of Engineering Science*, pp. 1–14, 2014.

[27] C. Schuster, B. Zhang, R. Vaish, P. G. P. o. the, and 2014, "RTI compression for mobile devices - IEEE Conference Publication," *ieeexplore.ieee.org*,

[28] F. Ponchio, M. Corsini, and R. Scopigno, "RELIGHT: A compact and accurate RTI representation for the web," *Graphical Models*, vol. 105, p. 101 040, Sep. 2019.

[29] K. Van Ngo, J. J. Storvik, C. A. Dokkeberg, I. Farup, and M. Pedersen, "QuickEval: a web application for psychometric scaling experiments," in *Image Quality and System Performance XII*, M.-C. Larabi and S. Triantaphillidou, Eds., International Society for Optics and Photonics, Feb. 2015, 93960O.

[30] P. G. Engeldrum, ***Psychometric Scaling: A Toolkit for Imaging Systems Development***. Imcotek Pr; F First Edition Used edition, 2000.